



Critical REV Size of Multiphase Flow in Porous Media for Upscaling by Pore-Scale Modeling

Tong Liu¹ · Moran Wang¹

Received: 14 March 2021 / Accepted: 13 May 2021 / Published online: 25 May 2021
© The Author(s), under exclusive licence to Springer Nature B.V. 2021

Abstract

Digital rock analysis provides us a powerful tool for predicting geophysical properties and studying fluid and interfacial transport mechanisms in rocks. However, people have to struggle and find a balance between scanning resolution and sample size due to current limitations of imaging technologies. With satisfaction of resolution requirement, the sample size has to be larger than the critical size of representative element volume (REV), so that the consequent pore-scale models are able to provide meaningful geophysical predictions for upscaling to Darcy-scale analysis. Following our previous work [Energies, **11**: 1798, 2018] on REV size for single-phase flow, this work considers the critical size of REV for multiphase flow in porous media. A multiphase lattice Boltzmann model has been developed for simulation of two-phase immiscible flow. The relative permeability, which can be influenced by the capillary number and wettability, and the saturation of phases are calculated for upscaling. The critical size of REV for multiphase flow in porous media is therefore found and compared with that for single-phase flow. It is found that the REV size for the relative permeability–saturation curve of multiphase flow, which is influenced by the phase interaction and wettability, is beyond twice of that for the absolute permeability of single-phase flow in the present study.

Article Highlights

- The critical size of REV for multiphase flow in porous media is determined by pore-scale modeling.
- The REV size of multiphase flow is beyond twice that of single-phase flow on the same porous structure.
- The REV size for the relative permeability–saturation curve is influenced by the phase interaction and wettability.

Keywords Representative element volume · Upscaling · Relative permeability · Saturation · Pore-scale modeling

✉ Moran Wang
mrwang@tsinghua.edu.cn

¹ Department of Engineering Mechanics and CNMM, Tsinghua University, Beijing 100084, China

1 Introduction

Multiphase immiscible flow and displacement in porous media is a common phenomenon in nature and is of significance for many industrial issues, such as enhanced oil recovery, carbon dioxide storage, fuel cell, contaminant transport and groundwater remediation (Parlange 1980; Kang et al. 2010; Vilarrasa et al. 2010; Gharbi and Blunt 2012; Dai et al. 2014; Huppert and Neufeld 2014; Ha and Kim 2020; Aliseda and Heindel 2021). Traditionally, laboratory experiments have been conducted to study the transient and steady-state multiphase displacement process (Dullien and Dong 1996; Krevor et al. 2012; Akbarabadi and Piri 2013); however, those experiments can be very time-consuming and expensive and sometimes fail to reflect the real subsurface conditions. Besides, the interfacial transport and multiphase distribution patterns are essential for analyzing and modeling multiphase immiscible flow in porous media, which can be hardly observed through traditional laboratory experiments.

In recent years, the digital rock analysis has become a powerful tool to study multiphase displacement in rocks (Hughes and Blunt 2000; Blunt et al. 2013; Alpak et al. 2018; Chen et al. 2018). Utilizing developed imaging techniques such as X-ray computed tomography (CT), digital structures of real rocks are reconstructed and multiphase transport through digital rocks can be simulated with pore-scale simulations. Using direct numerical simulation (DNS) (Alpak et al. 2018), the interfacial transport and multiphase distribution patterns can be monitored through digital rock analysis and geophysical properties can be predicted. Though higher-resolution images can capture more detailed rock structures accompanied with more cost, smaller-size samples can be analyzed due to current limitations of imaging techniques. Researchers have been devoted to finding a balance between sample size and scanning resolution (Yoon and Dewers 2013; Liu et al. 2018; Mehmani et al. 2020). To provide meaningful geophysical predictions, sample size has to be larger than the representative elementary volume (REV) size with resolution requirement satisfied (Liu et al. 2018). REV is the smallest volume over which the measurement result is representative of the macroscopic property (Bear 1972). And it is essential to determine the REV size for upscaling pore-scale simulation results through digital rock analysis to make Darcy-scale predictions. Following the REV definition, the REV size can be determined through numerical studies on sample size effect with digital rock analysis. Mostaghimi et al. (2013) calculated the REV size for porosity and permeability of Berea sandstone. It was found that the REV size was different for porosity and permeability and the REV size for permeability was about twice larger than that for porosity. Liu et al. (2018) obtained the REV for porosity and permeability of tight sandstones. For tight sandstones, the REV size for permeability was about four times larger than that for porosity. Liu et al. (2021) also investigated the REV size for Bingham fluid flows and obtained the REV for effective permeability and pseudo start-up pressure gradient and found that the REV size was the same for a single-phase flow of Newtonian fluid and Bingham fluid.

To upscale the multiphase flow through porous media, the relative permeability is the key property to be considered. Relative permeability can be obtained through extension of the single-phase Darcy's law. Due to the viscous coupling effects (Bentsen 1998; Avraam and Payatakes 1999; Ayub and Bentsen 1999), the relative permeability are functions of many parameters including saturation, capillary number, viscosity ratio, and wettability. Among various DNS simulation methods, the lattice Boltzmann method (LBM) is a wise choice for its ease implementation for dealing with complex geometries and its solid derivation to the Navier–Stokes equation (NSE) (Chen and Doolen 1998; Wang et al. 2007a, b; Wang et al.

2007a, b). Through LBM simulations, the factors that influence the relative permeability have been thoroughly studied in the recent years (Dou and Zhou 2013; Zhao and Ning et al. 2017; Shi and Tang 2018; Zhao et al. 2018; Yi et al. 2019). Typical factors such as the contact angle, capillary number and viscosity ratio are studied for the two-phase immiscible flow in 2D square blocks (Dou and Zhou 2013), 2D rock slices (Zhao et al. 2017) and packed spheres (Shi and Tang 2018). Zhao et al. (2018) investigated the influence of wettability heterogeneity and proposed the flow tortuosity to characterize the complex flow path. Yi et al. (2019) studied effects of the surface roughness of fractures and found that the relative permeability was highly influenced by the fluid distribution pattern. Besides the above parameter studies, simulations in real rock samples have been also conducted. Jiang et al. (2017) calculated a three-phase relative permeability curve for Berea sandstone. Alpak et al. (2018) conducted simulations on a Gildehauser sandstone and obtained the relative permeability results compared with experiments.

Though the plenty works have been done on the relative permeability estimations, the REV size results for multiphase flow based on direct simulations, to the best knowledge of the authors, have not been reported. In this study, LBM is applied to study the sample size effect on an immiscible two-phase flow. The relative permeability is obtained after careful validations of the method. Considering the sample size effect, the REV size for multiphase flow is reported and compared with the single-phase flow in the same porous media.

2 Methods

2.1 Multiphase lattice Boltzmann model

In this work, the MRT (multirelaxation time) color-gradient LB model proposed (Xu et al. 2017; Xie et al. 2018a, b) is adopted. In this model, the two immiscible fluids (red and blue) are represented by the distribution functions f_i^r and f_i^b , respectively. The total distribution function is defined as $f_i = f_i^r + f_i^b$, which undergoes a collision as

$$f_i^* (\vec{x}, t) = f_i (\vec{x}, t) + \Omega_i (\vec{x}, t) + f_{F,i}, \tag{1}$$

where $f_i (\vec{x}, t)$ is the total distribution function in the i -th velocity direction at the position \vec{x} and time t , f_i^* is the post-collision total distribution function, Ω_i is the collision operator, and $f_{F,i}$ is the forcing term.

To reduce the unphysical spurious velocities (Yu and Fan 2010) and enhance the numerical stability (d’Humières, Ginzburg et al. 2002), the MRT scheme is chosen instead of the BGK approximation (Guo et al. 2019). With the MRT scheme, the collision operator Ω_i is given by

$$\Omega_i (\vec{x}, t) = -\mathbf{M}^{-1} \mathbf{S} \mathbf{M} (f_i (\vec{x}, t) - f_i^{eq} (\vec{x}, t)), \tag{2}$$

where f_i^{eq} is the equilibrium distribution function, \mathbf{M} is the transformation matrix, and \mathbf{S} is the diagonal relaxation matrix. The equilibrium distribution function f_i^{eq} is obtained by expanding the Maxwell–Boltzmann distribution in Taylor series of the local fluid velocity \vec{u} up to the second order:

$$f_i^{eq} = \rho \omega_i \left[1 + 3 \frac{\vec{c}_i \cdot \vec{u}}{c^2} + \frac{9}{2} \frac{(\vec{c}_i \cdot \vec{u})^2}{c^4} - \frac{3}{2} \frac{\vec{u} \cdot \vec{u}}{c^2} \right], \tag{3}$$

where \vec{c}_i is the discrete velocity in i -th direction, ω_i is the weight factor, and $\rho = \rho^r + \rho^b$ is the total density with ρ^r and ρ^b being the densities of red and blue fluids, respectively. For the two-dimensional nine-speed (D2Q9) model used in this study, the discrete velocity \vec{c}_i is given as

$$\vec{c}_i = \begin{pmatrix} 0 & c & 0 & -c & 0 & c & -c & -c & c \\ 0 & 0 & c & 0 & -c & c & c & -c & -c \end{pmatrix}, i = 0, 1, \dots, 8 \tag{4}$$

where $c = \delta x / \delta t$ with the lattice spacing δx and time step δt defined as 1 lu and 1 ts (lu, ts, and mu refer to LBM lattice length units, time step, and mass units, respectively) (Sukop and Or 2004); the weight factor ω_i is given by

$$\omega_i = \begin{cases} 4/9, & i = 0 \\ 1/9, & i = 1, 2, 3, 4 \\ 1/36, & i = 5, 6, 7, 8 \end{cases} \tag{5}$$

The transformation matrix M is explicitly given as

$$M = \begin{pmatrix} 1 & 1 & 1 & 1 & 1 & 1 & 1 & 1 & 1 \\ 0 & 1 & 0 & -1 & 0 & 1 & -1 & -1 & 1 \\ 0 & 0 & 1 & 0 & -1 & 1 & 1 & -1 & -1 \\ -4 & -1 & -1 & -1 & -1 & 2 & 2 & 2 & 2 \\ 4 & -2 & -2 & -2 & -2 & 1 & 1 & 1 & 1 \\ 0 & 1 & -1 & 1 & -1 & 0 & 0 & 0 & 0 \\ 0 & 0 & 0 & 0 & 0 & 1 & -1 & 1 & -1 \\ 0 & -2 & 0 & 2 & 0 & 1 & -1 & -1 & 1 \\ 0 & 0 & -2 & 0 & 2 & 1 & 1 & -1 & -1 \end{pmatrix} \tag{6}$$

The diagonal relaxation matrix S is defined as

$$S = \text{diag}[s_0, s_1, s_2, s_3, s_4, s_5, s_6, s_7, s_8], \tag{7}$$

where s_i is the relaxation rate for each distribution function f_i . The parameters s_0, s_1 and s_2 are the relaxation rates associated with the conserved moments such as the density and momentum and are chosen $s_0 = s_1 = s_2 = 0$. s_5 and s_6 are related to the kinematic viscosity ν by

$$s_5 = s_6 = \frac{1}{\tau} \text{ and } \nu = \frac{1}{3} \left(\tau - \frac{1}{2} \right) c^2 \delta t \tag{8}$$

Following the previous work (Pan et al. 2006), we choose $s_3 = s_4 = s_7 = s_8 = 8(2 - s_5) / (8 - s_5)$ to ensure numerical stability and avoid influence of varying relaxation time τ .

In this study, both red and blue fluids have equal densities, which are given as unity. To account for the unequal viscosities of the two fluids, the harmonic mean that ensures a constant viscous stress across the interface is used to determine the viscosity of the fluid mixture at the interface (Liu et al. 2014):

$$\frac{1}{\nu} = \frac{1 + \rho^N}{2} \frac{1}{\nu^r} + \frac{1 - \rho^N}{2} \frac{1}{\nu^b}, \tag{9}$$

where ν^r and ν^b are the kinematic viscosities of the red and blue fluids, respectively, and ρ^N is a color function used to identify the location of the interface, which is defined by

$$\rho^N = \frac{\rho^r - \rho^b}{\rho^r + \rho^b} \tag{10}$$

The forcing term $f_{F,i}$ is introduced to realize the effect of interfacial tension in the mixed interfacial region as body force. In the MRT framework, the forcing term is given by (Guo and Zheng 2008)

$$f_{F,i} = M^{-1} \left(I - \frac{1}{2} S \right) M F_i, \tag{11}$$

where I is a 9×9 unit matrix, and F_i is given by

$$F_i = \omega_i \left[\frac{3}{c^2} (\vec{c}_i - \vec{u}) + 9 \frac{\vec{c}_i \cdot \vec{u}}{c^4} \vec{c}_i \right] \cdot \vec{F}_c \delta t \tag{12}$$

In the above equation, \vec{F}_c is the capillary force and can be expressed as

$$\vec{F}_c = \frac{1}{2} \sigma \kappa \nabla \rho^N, \tag{13}$$

based on the continuum surface force (CSF) model of Brackbill et al. (Brackbill, Kothe et al. 1992), where σ is the surface tension coefficient and κ is the local interface curvature. κ is calculated by

$$\kappa = -\nabla_s \cdot \vec{n}, \tag{14}$$

where $\nabla_s = (\mathbf{I} - \vec{n}\vec{n}) \cdot \nabla$ is the surface gradient operator and $\vec{n} = \nabla \rho^N / |\nabla \rho^N|$ is an inwardly directed unit vector perpendicular to the interface.

The fluid velocity is defined as

$$\rho \vec{u}(\vec{x}, t) = \sum_i \vec{c}_i f_i(\vec{x}, t) + \frac{\delta t}{2} \vec{F}_c(\vec{x}, t) \tag{15}$$

to correctly recover NSE with a spatially varying body force (Guo and Zheng 2008).

To minimize the discretization errors, the compact finite difference stencil is used to evaluate the partial derivatives involved in the normal vector and the interface curvature. Taking a variable ϕ as an example, its partial derivatives can be evaluated by

$$\frac{\partial \phi(\vec{x})}{\partial x_\alpha} = \frac{3}{c^2} \sum_i \omega_i \phi(\vec{x} + \vec{c}_i \delta t) c_{i,\alpha} \tag{16}$$

Although the forcing term generates an interfacial tension, it does not ensure the immiscibility of both fluids. To promote phase segregation and maintain a reasonable interface, the recoloring algorithm proposed by Latva-Kokko and Rothman (Latva-Kokko and Rothman 2005) is applied. This algorithm allows the red and blue fluids to mix moderately along the tangent of the interface and meanwhile keeps the color distribution symmetric with respect to the color gradient. As a result, it can further reduce spurious velocities and overcome the lattice pinning problem arising in the original recoloring algorithm of Gunstensen et al. (Gunstensen, Rothman et al. 1991). The recolored distribution functions of the red and blue fluids, i.e., f_i^{r+} and f_i^{b+} , are

$$\begin{aligned} f_i^{r+}(\vec{x}, t) &= \frac{\rho^r}{\rho} f_i^*(\vec{x}, t) + \beta \frac{\rho^r \rho^b}{\rho} \omega_i \cos \varphi_i \\ f_i^{b+}(\vec{x}, t) &= \frac{\rho^b}{\rho} f_i^*(\vec{x}, t) - \beta \frac{\rho^r \rho^b}{\rho} \omega_i \cos \varphi_i \end{aligned} \tag{17}$$

where $\beta(0 \leq \beta \leq 1)$ is a free parameter related to the interface thickness and is set to be 0.7 in this study; φ_i is the angle between the color gradient $\nabla \rho^N$ and the discrete velocity \vec{c}_i , which is given by

$$\cos \varphi_i = \frac{c_i \cdot \nabla \rho^N}{|c_i| |\nabla \rho^N|} \tag{18}$$

After the recoloring step, the distribution functions of red and blue fluids both propagate to the neighboring lattice sites, which is known as the propagation or streaming step:

$$f_i^{k+}(\vec{x} + \vec{c}_i \delta t, t + \delta t) = f_i^{k+}(\vec{x}, t), k = rorb \tag{19}$$

with the post-propagation distribution functions being used to calculate the density of each fluid by $\rho^k = \sum_i f_i^k$.

2.2 Wetting Boundary Condition

The geometrical formulation (Xu, Liu et al. 2017) is used to directly modifying the orientation of the color gradient $\nabla \rho^N$ at the contact lines such that it matches the desired contact angle θ . To accomplish this scheme, ρ^N in the wall nodes is pre-estimated through a weighted average of its nearest ρ^N in fluid nodes, which is given by

$$\rho^N(\vec{x}) = \frac{\sum_{i:\vec{x}+\vec{c}_i\Delta t \in C_F} \omega_i \rho^N(\vec{x}+\vec{c}_i\Delta t)}{\sum_{i:\vec{x}+\vec{c}_i\Delta t \in C_F} \omega_i}, \vec{x} \in C_S \tag{20}$$

where C_F and C_S represent set of the fluid nodes and wall nodes.

With the values of ρ^N obtained, the color gradient $\nabla \rho^N$ in all fluid nodes can be directly computed, while it does not necessarily match with the desired contact angle in the pore nodes near the wall. Color gradient in these nodes, denoted by $\nabla \rho^{N*}$, is modified by changing the orientation of the $\nabla \rho^{N*}$ while keeping its magnitude the same. For 2D cases, two possible orientation of color gradient can be determined by the unit normal vector of the solid surface \vec{n}_w and contact angles θ as

$$\begin{aligned} \vec{n}_1 &= (n_{w,x} \cos \theta - n_{w,y} \sin \theta, n_{w,y} \cos \theta + n_{w,x} \sin \theta) \\ \vec{n}_2 &= (n_{w,x} \cos \theta + n_{w,y} \sin \theta, n_{w,y} \cos \theta - n_{w,x} \sin \theta) \end{aligned} \tag{21}$$

where $n_{w,x}$ and $n_{w,y}$ are the x and y components of \vec{n}_w . To choose an appropriate theoretical unit normal vector, Euclidean distances D_1 and D_2 are computed by

$$\begin{aligned} D_1 &= |\vec{n}^* - \vec{n}_1| \\ D_2 &= |\vec{n}^* - \vec{n}_2| \end{aligned} \tag{22}$$

The unit normal vector of the interface \vec{n} is then selected by

$$\vec{n} = \begin{cases} \vec{n}_1 & D_1 < D_2 \\ \vec{n}_2 & D_1 > D_2 \\ \vec{n}_w & D_1 = D_2 \end{cases} \tag{23}$$

Finally, the modified color gradient $\nabla\rho^N$ is obtained by

$$\nabla\rho^N = \left| \nabla\rho^{N*} \right| \vec{n} \tag{24}$$

2.3 Model Validation

To validate the accuracy of the model we adopt, the layered two-phase flows under different fluid saturations in a 2-D horizontal channel are simulated by this model and the simulation results are compared with the theoretical solutions. Non-dimensional settings are adopted in the present study. Transformations between the physical unit and the lattice unit are accomplished with $\rho^{LBM} = \rho/\rho_c$, $v^{LBM} = v/(l_c/t_c)$, $\sigma^{LBM} = \sigma/(\rho_c l_c/t_c^2)$, $u^{LBM} = u/(l_c/t_c)$ and $p^{LBM} = p/(\rho_c l_c^2/t_c^2)$. Here, $\rho_c = 1\text{kg/m}^3$, $l_c = \delta x$ is the lattice spacing, $t_c = \delta t$ is the time step. Lattice spacing is determined by the physical structure size and the domain size. Time step is determined by the lattice spacing and the physical viscosity with Eq. (8). The simulation domain is shown in Fig. 1, and the size of the domain is 100×100 . The wetting fluid flows along the solid walls, while the non-wetting fluid flows in the center of the channel. The flow is driven by a constant body force G in x direction and periodic boundary condition is applied in this direction. Periodic boundary condition means when the fluid exits from one end, it will reenter the simulation domain from the other end. Assuming the flow in the channel is a Poiseuille type, the analytical solution for the velocity profile can be obtained as (Ba, Liu et al. 2016)

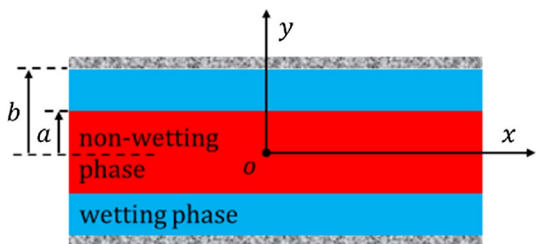
$$u_x(y) = \begin{cases} \frac{G}{2\mu_w}(b^2 - y^2) & a < y < b \\ \frac{G}{2\mu_n}(a^2 - y^2) + \frac{G}{2\mu_w}(b^2 - a^2) & 0 < y \leq a \end{cases}, \tag{25}$$

where μ_w and μ_n are the dynamic viscosity of the wetting and non-wetting phases. Relative permeability of the wetting phase (k_{rw}) and non-wetting phase (k_{rn}) can then be calculated based on the velocity profile as (Yiotis, Psihogios et al. 2007)

$$k_{rn} = (1 - S_w) \left[\frac{3}{2}M + (1 - S_w)^2 \left(1 - \frac{3}{2}M \right) \right], \tag{26}$$

$$k_{rw} = \frac{1}{2}S_w^2(3 - S_w)$$

Fig. 1 Schematic plot of computation domain for 2D layered flow



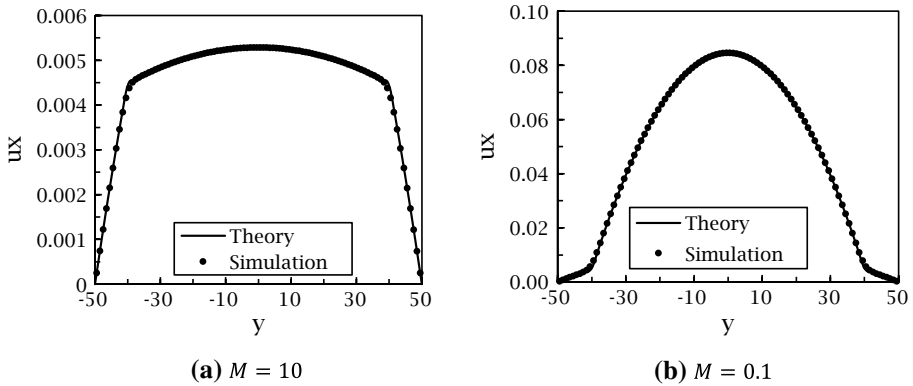


Fig. 2 Result of velocity profile for layered flow at $S_w = 0.2$ for **a** $M = 10$ and **b** $M = 0.1$

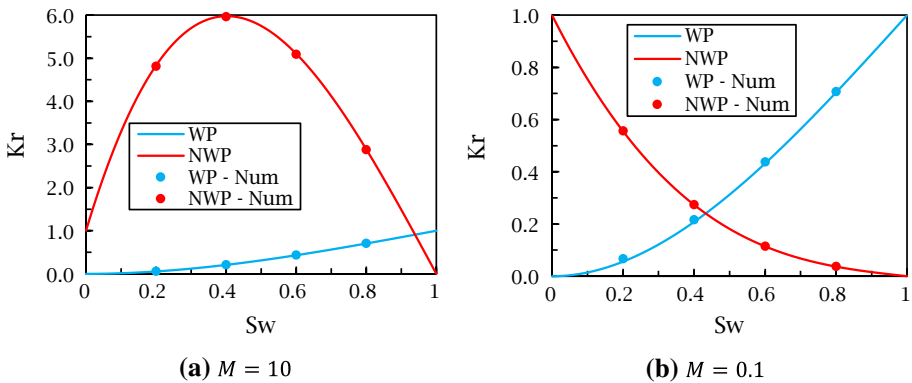


Fig. 3 Result of relative permeability–saturation curve for layered flow at **a** $M = 10$ and **b** $M = 0.1$. “Num” in legend represents numerical results

where $S_w = 1 - a/b$ is the saturation of wetting phase, $S_n = a/b$ is the saturation of non-wetting phase, and $M = \mu_n/\mu_w$ is the dynamic viscosity ratio. Two different fluid systems are adopted here: one is $M = 10$ with $\rho_w = \rho_n = 1$, $v_n = 2.0$ and $v_w = 0.2$ and the other one is $M = 0.1$ with $\rho_w = \rho_n = 1$, $v_n = 0.2$ and $v_w = 2.0$. The velocity distributions with the wetting fluid saturation of 0.2 and the relative permeability–saturation curves are obtained, as shown in Figs. 2 and 3, respectively. Both the velocity distribution and the relative permeability curve match very well with the theoretical solutions. Especially for the case of $M = 10$, the relative permeability of non-wetting phase shows a non-monotonic change with saturation due to the lubrication effect (Dou and Zhou 2013).

To validate the wetting boundary condition, equilibrium distributions of wetting and non-wetting fluid column placed in a 2D capillary tube are investigated. The simulation domain is shown in Fig. 4, and the size of the domain is 300×100 . The red column is placed in the center and blue fluid in the rest of the domain. Solid walls are placed on both up and down boundaries and periodic boundary conditions are applied for left and right boundaries. The parameters are fixed as $\rho^r = \rho^b = 1.0$, $v^r = v^b = 1/6$ and $\sigma = 0.01$.



Fig. 4 Equilibrium distribution of fluid column in capillary tube for **a** $\theta = 150^\circ$ and **b** $\theta = 30^\circ$

The prescribed contact angle varies from 30° to 150° and simulated contact angle is evaluated using the following geometrical relation (Akai, Bijeljic et al. 2018):

$$\theta = \pi/2 - 2 \arctan [W/H], \quad (27)$$

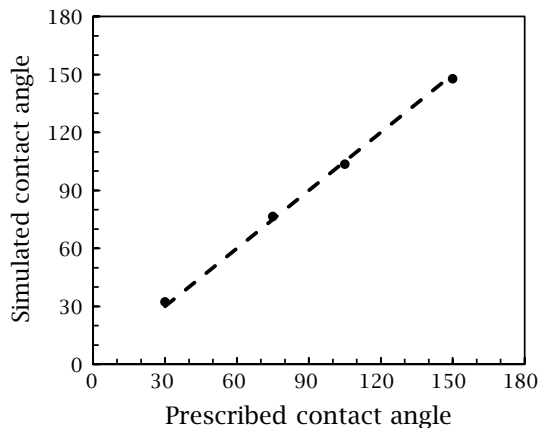
where θ is the contact angle, H is the half width of the capillary tube, and W is the height of the meniscus. Comparison between the prescribed contact angle and the resultant simulated contact angle is shown in Fig. 5.

2.4 Simulation Process

A 2D random structure is generated by randomly placed balls. The ball diameter is 80 and a minimal distance between each ball is specified as 2 to avoid ball interaction. The domain size of the generated sample is 3000×3000 and the pore size distribution is shown in Fig. 6. Porosity of the generated sample is 56.4% and the mean pore size is 33.

To investigate the sample size effect, sub-samples with square shape are cropped from the generated sample with fixed square center as shown in Fig. 7. Ten sub-samples with size changing from 200 to 2000 are cropped, and the size spacing is 200. Porosity ϕ and specific area s of sub-samples are calculated, and reciprocal of s is used to characterize the average pore size. When sample size changes, porosity ϕ and reciprocal of specific area $1/s$ also change. However, the deviation caused by sample size change is very small, which is shown in Fig. 8. By specifying the tolerance of variance as 10%, REV of ϕ and $1/s$ are found both to be 200.

Fig. 5 Comparison of the prescribed contact angle and simulated contact angle (circles) for fluid column in capillary tube



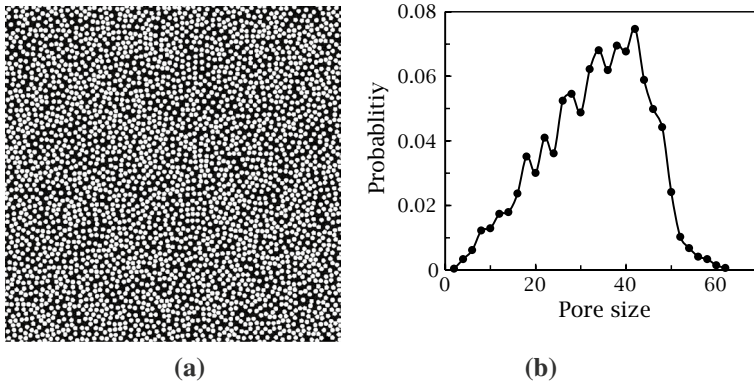


Fig. 6 **a** Generated 2D porous structure by randomly placed balls. **b** Pore size distribution of the generated porous structure with characteristic pore diameter $d_c = 42$

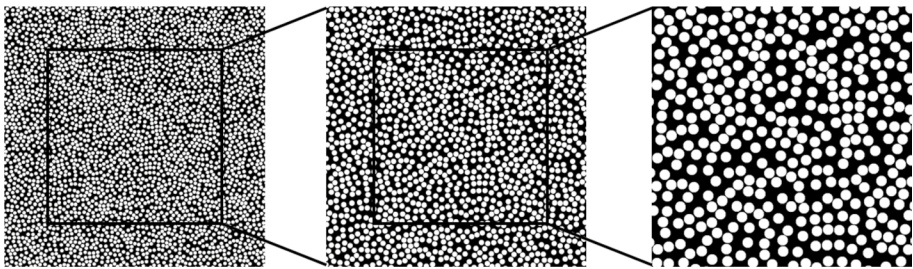


Fig. 7 Varying size structures cropped from generated porous structure. Sample size is 3000, 2000 and 1000 from left to right. Pores are shown in black and solid in white

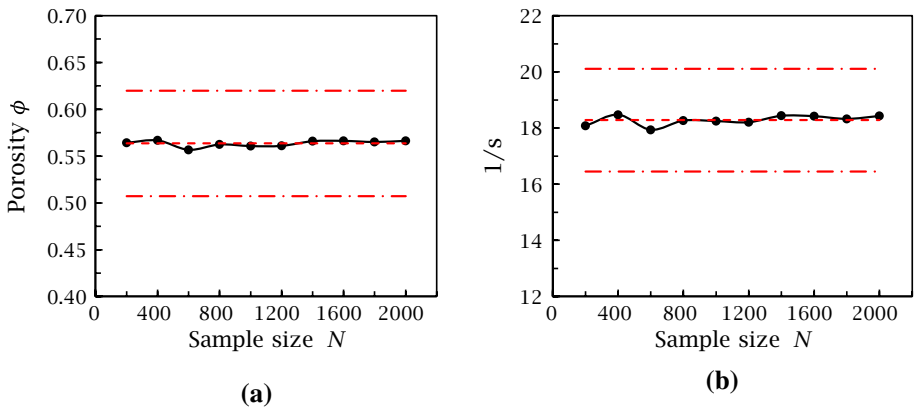


Fig. 8 Results of **a** porosity ϕ and **b** reciprocal of specific area $1/s$ change with sample size N . Short dashed line represents the mean property, and long dashed line covers 10% variation from the mean

Note that there are two different ways to choose sub-size samples when studying REV effect. One is changing sample size while fixing the sample center (Liu, Jin et al. 2018), as this work has applied. The other one is randomly choosing sample positions (Mostaghimi, Blunt et al. 2013). Advantage of second way is that several sub-size samples can be chosen and coefficient of variance can be obtained to display the statistical deviation. However, number of sub-size samples that can be chosen is decreasing with increasing sample size, since overlap is avoided between sub-size samples. This means that when sample size reaches REV, it is highly likely that still only one sub-size sample can be chosen. When sample size does not reach REV, sample number and coefficient variance can provide some confidence on the mean property at that sample size, but this confidence has little meaning, since the mean property will not match property at REV until sample size is enlarged to REV size no matter how many sub-size samples you can obtain. In our understanding, it is not necessary to choose several sub-size samples and calculate coefficient of variance when investigating REV size from one raw sample. The sample-dependent or position-dependent effect can only be studied with several raw samples, and REV needs to be satisfied for each sample. Thus, the first one is preferred to study REV size from one raw sample, and this way also matches the REV definition proposed by Bear (Bear 1972).

Permeability of sub-samples are calculated. The up and down bounds are set as fixed wall, and left and right bounds are set as inlet and outlet. Fixed pressure as set at inlet and outlet with certain pressure difference Δp . The extrapolation scheme (Guo, Zheng et al. 2002) is used for pressure boundary, and bounce-back is used for wall boundary. The pressure gradient is fixed as $\Delta p/N = 1 \times 10^{-6}$, so the pressure difference changes when sample size changes. For example, Δp is set to be 2×10^{-3} for sample $N = 2000$. The density is set as $\rho = 1$ and viscosity as 0.2. We check the Reynolds number at size $N = 2000$ and find that $Re = Qd/Av \sim 10^{-6}$, which guarantees that inertial effect makes little difference and Darcy's law is applied to calculate permeability

$$k = \frac{\mu Q}{\Delta p N} \quad (28)$$

With the velocity distribution obtained after simulation, the tortuosity of permeability is also calculated with

$$\tau = \frac{\langle |u| \rangle}{\langle u_x \rangle}, \quad (29)$$

where $\langle |u| \rangle$ is the value of average velocity magnitude and $\langle u_x \rangle$ is the value of average velocity in x direction.

Results of permeability k and tortuosity τ changing with sample size N are shown in Fig. 9. The REV for permeability k and for tortuosity τ can be obtained as 1200 and 200, respectively.

To calculate the relative permeability, the following procedure is applied. Firstly, imbibition process is simulated. Inlet buffer and outlet buffer are added to the porous structure with size 40 and 20, respectively. Porous structure and outlet are saturated with non-wetting phase, and the inlet is saturated with the wetting phase. The up and down bounds are set as fixed wall, and the contact angle is the same with that of the sample. Fixed velocity is applied at inlet so that wetting phase is displaced into the sample. Parameters are set as $\rho_w = \rho_n = 1$, $v_w = v_n = 0.2$, $\sigma = 0.01$ and $\theta = 60^\circ$. The injection velocity is fixed as $u_{in} = 1 \times 10^{-4}$ and the capillary number is calculated as $Ca = \mu_w u_{in} / \sigma = 2 \times 10^{-3}$. Simulation is terminated after 1 PV (pore volume) wetting phase is injection into the sample.

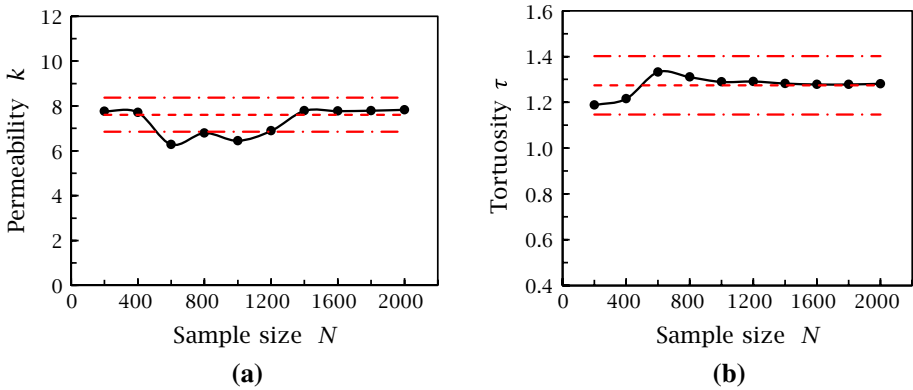


Fig. 9 Results of **a** permeability k and **b** tortuosity τ change with sample size N . Short dashed line represents the mean property, and long dashed line covers 10% variation from the mean

With the intermediate results extracted, the phase distribution with a varying saturation can be obtained and used as the initial phase distribution for relative permeability calculation. For the saturation calculation, inlet and outlet are cut off and only the phase distribution in the porous structure is counted. To exclude influence of capillary pressure gradient and saturation gradient, external force $G = 1 \times 10^{-6}$ is applied to drive the fluid system. The sample is mirrored as well as the phase distribution to ensure that periodic condition can be applied; thus, the saturation keeps constant in the simulation. For this simulation, capillary number can be characterized as $Ca = kG/\sigma \sim 8 \times 10^{-4}$. Relative permeability of wetting and non-wetting phases is then calculated by

$$k_{rw} = \frac{u_{x,w}}{u_D}, \quad k_{rn} = \frac{u_{x,n}}{u_D}, \tag{30}$$

where $\langle u_{x,w} \rangle$ and $\langle u_{x,n} \rangle$ is the value of average velocity in x direction of wetting and non-wetting phases and u_D is the Darcy velocity at same external force, which can be calculated by $u_D = kG/\mu_w$.

3 Results and discussion

3.1 Sample size effect on relative permeability

Considering imbibition process at sample size $N = 1200$, phase distributions at varying saturation are shown in Fig. 10. Flat advancing front is observed and displacing phase (blue wetting phase) is well connected, while isolated clusters of displaced phase (red non-wetting phase) exist when S_w gets high. These distributions are used as initial phase distribution for relative permeability calculation. Take $S_w = 0.5$ for an example, average velocities of each phase changes with time iteration are given in Fig. 11 and phase distributions at initial state and stable flowrate state are shown in Fig. 12. Though isolated clusters of each phases exist, most parts are connected with each other. Since periodic condition is applied at left and right boundaries, flow process simulated during relative permeability calculation mimics the displacement of two fluid columns in a tube under external body force. In that

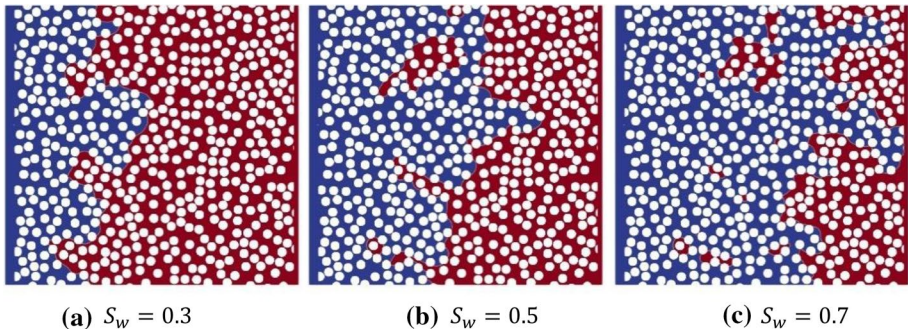


Fig. 10 Results of phase distributions at varying saturations. Obtained from imbibition process simulation at sample size $N = 1200$

Fig. 11 Results of $\langle u_{x,n} \rangle$ at sample size $N = 1200$. Initial distribution is obtained from imbibition process at $S_w = 0.5$

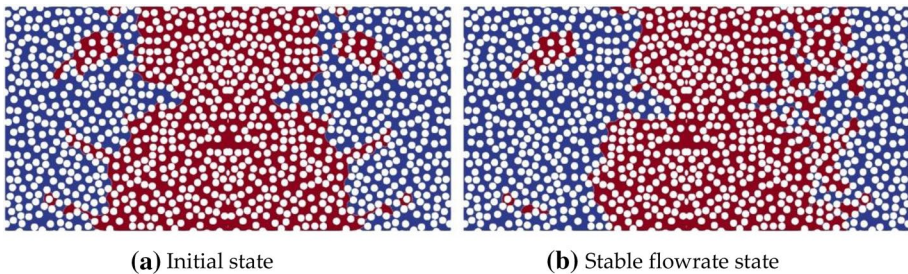
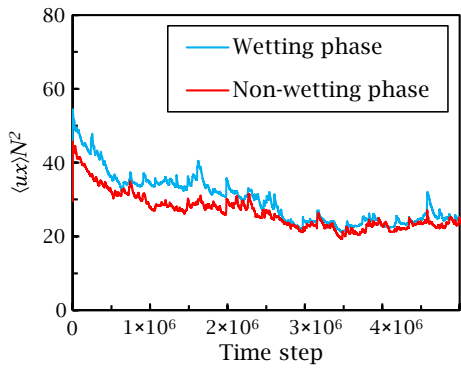


Fig. 12 Results of phase distributions at initial state and stable flowrate state. Sample size is $N = 1200$ and saturation is $S_w = 0.5$

case, displacing velocity for each phase is almost same and $\langle u_x \rangle$ is only related to saturation of each phase. For $S_w = 0.5$, it is observed that $\langle u_{x,w} \rangle$ and $\langle u_{x,n} \rangle$ are almost the same when flowrate gets stable.

When the flowrate gets stable, the relative permeability can be calculated following Eq. (30). In practice, the average of the last 1/5 stable period is used to exclude the deviation. Results of the relative permeability at $S_w = 0.5$ changing with sample size are shown

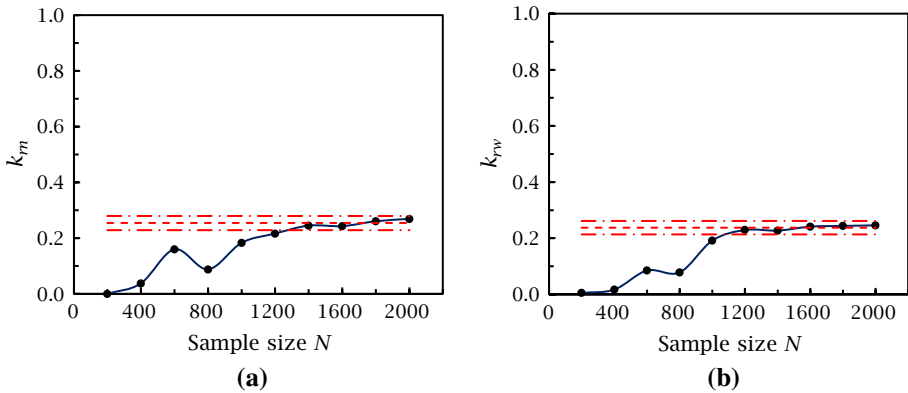
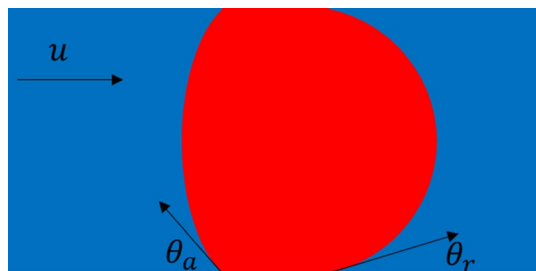


Fig. 13 Results of **a** non-wetting phase and **b** wetting phase relative permeability at varying sample size N at saturation $S_w = 0.5$. Short dashed line represents the mean property, and long dashed line covers 10% variation from the mean

in Fig. 13. It is observed that the relative permeability tends to increase as the sample size increases, and it finally keeps stable after some deviation. Though k_m still increases a little bit when the sample size reaches 2000, the deviation is within the variation limit 10% and the REV size of k_m and k_{rw} are calculated. For the wetting phase, the REV size for relative permeability is 1200, which is the same with that of absolute permeability. For the non-wetting phase, the REV size for relative permeability is 1400, which is larger than that of permeability. The result confirms the existence of a REV for relative permeability and shows that the REV size is different for wetting phase and non-wetting phase.

To explain the increasing tendency of relative permeability with sample size, we consider fluid columns displacement shown in Fig. 14. Different from Fig. 4b, in which each phase is in equilibrium and the contact angle is a static contact angle, the contact angle hysteresis should be considered to mimic two-phase flow in porous media. The contact angle hysteresis comes from the geometry effect of pore space. When the two-phase interface goes from pore to throat or goes from throat to pore, the capillary pressure changes due to the pore size changes and geometry changes [29]. To consider these effects and reduce the model to fluid column displacement, the contact angle hysteresis is used to model the apparent capillary pressure. In such a model, the external force tries to overcome the capillary resistance to get the columns move. The external force, expressed as GN , is proportional to sample size. When the sample size is small, the fluid columns cannot move since the capillary force dominates flow. When the sample size gets larger, the influence of

Fig. 14 Schematic plot of fluid columns displacement in a tube



capillary resistance gets smaller, the viscous force gradually dominates flow and then the flow approaches a single-phase flow. This explains the increase tendency of relative permeability with sample size.

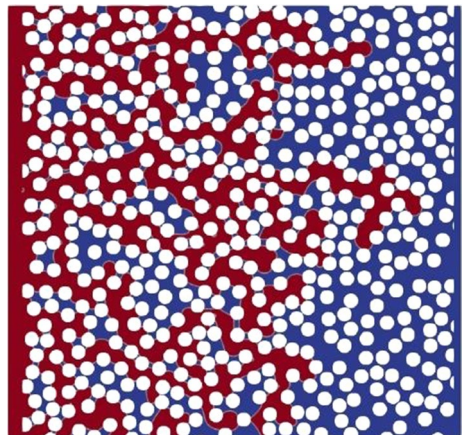
According to the above analysis, the relative permeability will approach saturation of each phase when the sample size is large enough, since the capillary force is small and the flow of each phase approaches single-phase flow in the above model. However, the relative permeability of each phase obtained from Fig. 14 is about 0.3, far from saturation 0.5. This decrease comes from the isolated clusters formed during displacement. These clusters occupy certain saturation, on the one hand, and block the flow path, on the other hand. So the relative permeability is usually smaller than the saturation of that phase. And due to the small clusters influence on saturation and flow path, the REV size of relative permeability is usually larger than that of permeability.

3.2 Influence of Wettability

The above analysis on REV size for relative permeability of imbibition process indicates that the phase connectivity is quite important. Since the wettability directly influences the distribution pattern in imbibition and drainage process, the influence of wettability is checked. For a contact angle at $\theta = 60$, the drainage process is simulated to obtain the initial phase distribution by displacing a wetting phase with a non-wetting phase. When the sample size is $N = 1200$, the phase distributions at $S_w = 0.5$ of drainage process are shown in Fig. 15. Compared with imbibition process, it can be seen that the advancing front is twisted. Due to the unstable advancing front, more isolated wetting phase cluster forms during drainage.

Still at the saturation $S_w = 0.5$, the relative permeability is calculated at varying sample sizes. The results are shown in Fig. 16. As the sample size changes, similar tendency is observed for k_{rn} and the REV size is obtained as 1200. For a wetting phase, the relative permeability tends to increase with the sample size and the REV size is beyond 2000. Thus, different from the imbibition process, the REV size for k_{rw} is larger than that of k_{rn} for drainage process. It is believed that this small REV size is a result of the big connected fluid clusters.

Fig. 15 Results of phase distributions at varying saturations. Obtained from drainage process simulation at sample size $N = 1200$



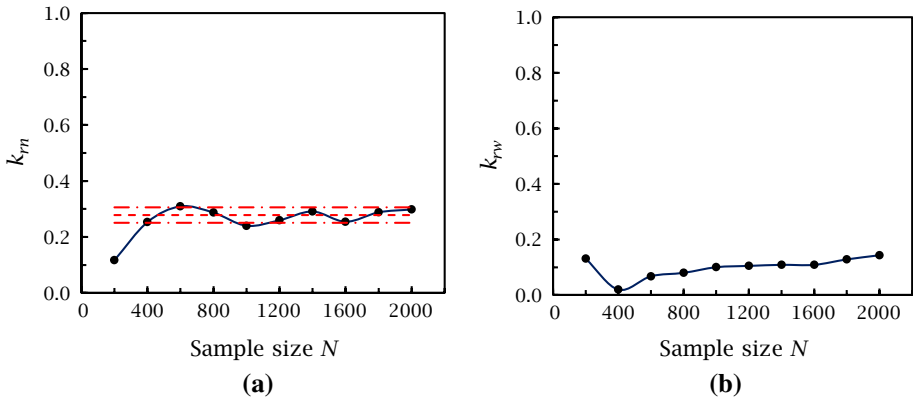


Fig. 16 Results of **a** non-wetting phase and **b** wetting phase relative permeability at varying sample size N at saturation $S_w = 0.5$ for drainage process. Short dashed line represents the mean property, and long dashed line covers 10% variation from the mean

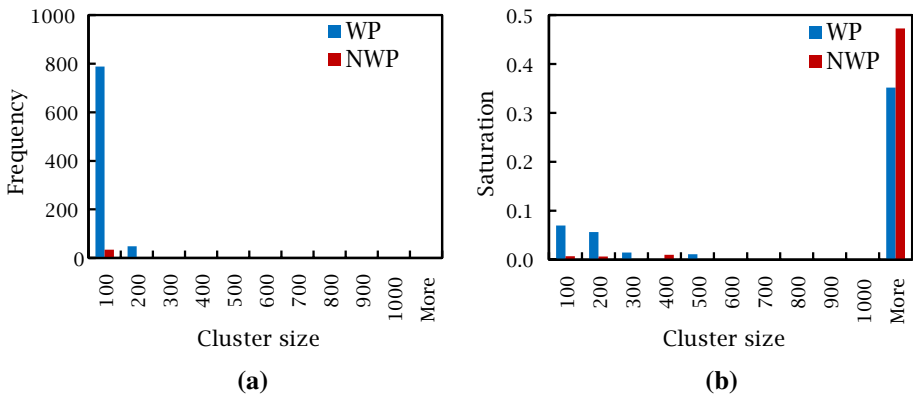


Fig. 17 Histogram of cluster size at sample size $N = 2000$ and saturation $S_w = 0.5$ for drainage process

Since the cluster size and the saturation play important roles, analysis has been conducted on the cluster size distribution. As shown in Fig. 17, many isolated clusters of wetting phase exist and occupy about 15% of saturation. For a non-wetting phase, one large cluster occupies most of saturation. Saturations of the largest size cluster are extracted, and the sample size influence on it is shown in Fig. 18. For a non-wetting phase, saturation of the largest size clusters is almost the total saturation when the sample size reaches 1200, which is exactly the REV size of k_{rn} . For a wetting phase, the saturation of largest size clusters decreases when the sample size increases. After a stable stage from 1000 to 1600, the saturation increases a little at $N = 1800$ and 2000. It can be found that the relative permeability k_{rw} goes through a similar tendency when the sample size increases. This confirms the above analysis on relative permeability of imbibition process that the largest connected cluster is the most important for relative permeability. When the sample size gets large and the capillary resistance gets small compared to the external force, the cluster saturation of the largest size influences changes of the relative permeability.

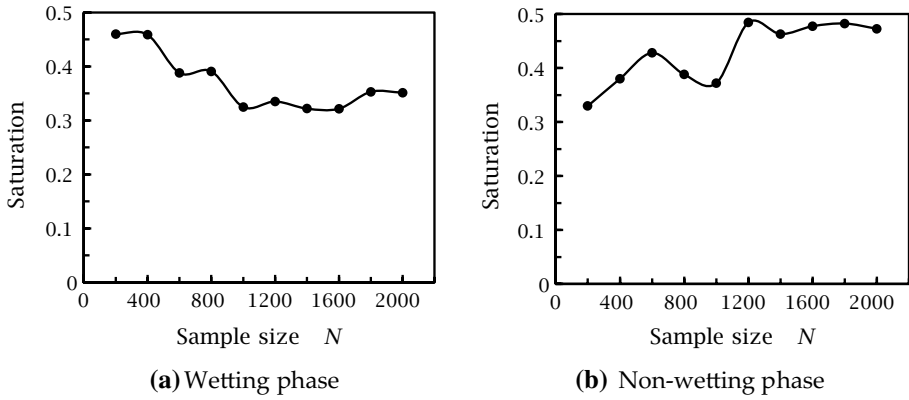


Fig. 18 Sample size influence on largest size cluster saturation at saturation $S_w = 0.5$ for drainage process

3.3 Influence of Saturation and Comparison with REV Size for Absolute Permeability

The above results confirm the existence of REV size for relative permeability at a certain saturation. In industry applications, the saturation of samples distributes among a range and the relative permeability–saturation curve is needed to upscale simulations for multiphase flows, instead of a relative permeability at a single saturation. Since the REV size of permeability is usually easier to find, comparison of REV sizes between of the absolute permeability and of the relative permeability–saturation curve is very important (Fig. 19).

Besides $S_w = 0.5$, two other saturations, 0.3 and 0.7, are also chosen to investigate the influence of saturation. The results are shown in Fig. 15, and the calculated REV size is listed in Table 1. It is observed that the saturation will influence the REV size for k_{rn} or k_{rw} . If we consider the largest REV size at varying S_w for k_{rn} and k_{rw} as the REV size for relative permeability–saturation curve, the REV size is beyond 2000, which is much large than that of absolute permeability (around 1200 on the same structure). The reason

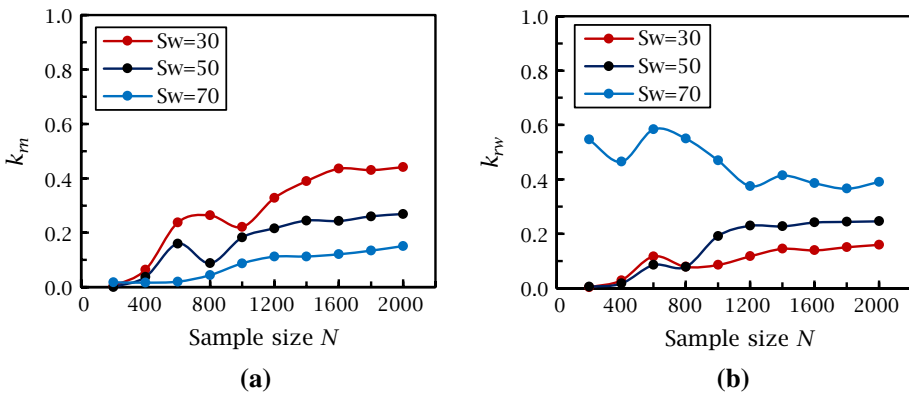


Fig. 19 Results of **a** non-wetting phase permeability (k_{rn}) and **b** wetting phase relative permeability (k_{rw}) change with structure size N at varying saturation S_w . In legend, saturation is shown in percentage

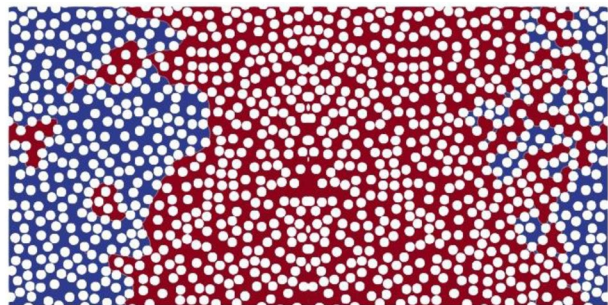
Table 1 REV at varying saturation for relative permeability of wetting phase (k_{rw}) and non-wetting phase (k_{rn})

S_w	k_{rn}	k_{rw}
0.3	1600	1400
0.5	1400	1200
0.7	> 2000	1200

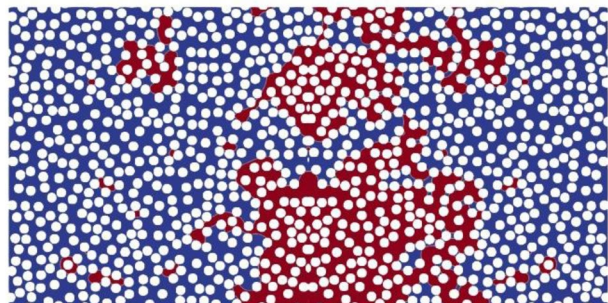
to this large REV size is that saturation occupied by small clusters of the non-wetting phase is comparable to S_n when $S_w = 0.7$. Figure 16 shows the phase distributions at a stable flowrate state when the sample size is $N = 1200$ and the saturation is $S_w = 0.3$ and 0.7. It can be seen that the wetting phase is well connected at $S_w = 0.3$ while the non-wetting phase is poorly connected at $S_n = 0.3$ ($S_w = 0.7$) (Fig. 20). Since the initial phase distributions come from imbibition process, the REV size for relative permeability–saturation curve is mainly influenced by REV for k_{rn} at high S_w .

Although the simulations are conducted on simple 2D structures, the characteristics of drainage and imbibition processes are well captured on the advancing front and the isolated clusters. For more complex structures, differences may exist in the distributions of number and saturation of the isolated clusters. In those cases, similar analysis can be conducted on the relation of relative permeability and the clusters distributions. Since more isolated clusters exist in more complex structures, saturation of largest size cluster may rely on larger sample size to reach stable and thus leads to larger REV of relative permeability.

Fig. 20 Results of phase distributions at stable flowrate state at saturation $S_w = 0.3$ and 0.7. Sample size is $N = 1200$. **a** $S_w = 0.3$ **b** $S_w = 0.7$



(a) $S_w = 0.3$



(b) $S_w = 0.7$

As for the influence of capillary number, which can be defined as $Ca = kG/\sigma$, its influence can be related to the influence of body force. From the above explanation on increasing tendency of relative permeability with sample size, it is known that the sample size needs to be large enough so that the driving force GN can overcome the capillary resistance (Wang et al. 2021). When the body force G gets smaller and the capillary number gets smaller, the capillary force becomes more important and the relative permeability gets smaller since the small-size fluid clusters fail to be moved (Shi and Tang 2018). The sample size needs to get larger to firstly overcome the capillary resistance, and a lower capillary number will lead to a larger REV size of relative permeability.

4 Conclusions

Digital rock analysis has become a powerful tool to predict geophysical properties and study fluid and interfacial transport mechanism in rocks. With the resolution requirement satisfied, the sample size has to be larger than the critical REV size to guarantee meaningful geophysical predictions. To upscale the multiphase flow in porous media, the sample size effect on relative permeability is studied with a multiphase LBM model and the REV size for relative permeability is reported. Main results of this work are summarized as follows:

- The pore-scale simulation results for both imbibition and drainage processes indicate that the fluid clusters are very important for the relative permeability analysis. Applying a constant pressure gradient, the smaller-size fluid cluster is more likely to be immobile. When the sample size gets larger, the larger-size mobile fluid clusters form and lead to an increase in relative permeability. When the saturation of these large-size clusters gets stable, the relative permeability also gets stable and the REV size is reached.
- The REV size for the relative permeability of multiphase flow is found to be larger than that for the absolute permeability of single-phase flow on the same porous structure. At a lower saturation, the small-size fluid clusters are not negligible and thus a larger sample size is required to reach REV. In the present work, the REV size for relative permeability–saturation curve is beyond twice of the REV size for absolute permeability.
- The REV size for relative permeability is influenced by both saturation and wettability and is different for wetting phase and non-wetting phase. It is found that the REV size for relative permeability of displacing phase is smaller than that of displaced phase for both drainage and imbibition processes at varying saturations.

Though a simple 2D structure is considered in this paper, the characteristics of multiphase flow on advancing front and isolated fluid clusters are well captured and the analysis based on fluid clusters can be applied to 3D complex structures with no more manual efforts.

Acknowledgements This work is financially supported by the National Key Research and Development Program of China (No. 2019YFA0708704) and NSF grant of China (No. U1837602). Our simulations are run on the “Explorer 100” cluster of Tsinghua National Laboratory for Information Science and Technology.

Author Contributions TL performed simulation and analysis of data and wrote the paper. MW provided guidance and critical review of the work.

Data Availability The original data are not available publicly online but can be provided by the authors for interested researchers.

Code Availability The source code is not available publicly online but can be provided by the authors for interested researchers.

Declarations

Conflict of interest The authors declare that they have no conflict of interest.

References

- Akai, T., Bijeljic, B., Blunt, M.J.: Wetting boundary condition for the color-gradient lattice boltzmann method: validation with analytical and experimental data. *Adv Water Resour* **116**, 56–66 (2018)
- Akbarabadi, M., Piri, M.: Relative permeability hysteresis and capillary trapping characteristics of supercritical CO₂/brine systems: an experimental study at reservoir conditions. *Adv Water Resour* **52**, 190–206 (2013)
- Aliseda, A., Heindel, T.J.: X-ray flow visualization in multiphase flows. *Ann Rev Fluid Mech* **53**(543), 567 (2021)
- Alpak, F.O., Berg, S., Zacharoudiou, I.: Prediction of fluid topology and relative permeability in imbibition in sandstone rock by direct numerical simulation. *Adv Water Resour* **122**, 49–59 (2018)
- Avraam, D.G., Payatakes, A.C.: Flow mechanisms, relative permeabilities, and coupling effects in steady-state two-phase flow through porous media, the case of strong wettability. *Ind. Eng. Chem. Res.* **38**(3), 778–786 (1999)
- Ayub, M., Bentsen, R.G.: Interfacial viscous coupling: a myth or reality? *J. Petrol. Sci. Eng.* **23**(1), 13–26 (1999)
- Ba, Y., Liu, H., Li, Q., Kang, Q., Sun, J.: Multiple-relaxation-time color-gradient lattice boltzmann model for simulating two-phase flows with high density ratio. *Phys. Rev. E* **94**(2), 023310 (2016)
- Bear, J.: *Dynamics of fluids in porous media*. Dover Publications, New York (1972)
- Bentsen, R.G.: Effect of momentum transfer between fluid phases on effective mobility. *J. Petrol. Sci. Eng.* **21**(1–2), 27–42 (1998)
- Blunt, M.J., Bijeljic, B., Dong, H., Gharbi, O., Iglauer, S., Mostaghimi, P., Paluszny, A., Pentland, C.: Pore-scale imaging and modelling. *Adv. Water Resour.* **51**, 197–216 (2013)
- Brackbill, J.U., Kothe, D.B., Zemach, C.: A continuum method for modeling surface-tension. *J. Comput. Phys.* **100**(2), 335–354 (1992)
- Chen, S., Doolen, G.D.: Lattice boltzmann method for fluid flows. *Annu. Rev. Fluid Mech.* **30**, 329–364 (1998)
- Chen, Y., Li, Y., Valocchi, A.J., Christensen, K.T.: Lattice Boltzmann simulations of liquid CO₂ displacing water in a 2D heterogeneous micromodel at reservoir pressure conditions. *J. Contam. Hydrol.* **212**, 14–27 (2018)
- Dai, Z., Middleton, R., Viswanathan, H., Fessenden-Rahn, J., Bauman, J., Pawar, R., Lee, S.-Y., McPherson, B.: An integrated framework for optimizing CO₂ sequestration and enhanced oil recovery. *Environ. Sci. Technol. Lett.* **1**(1), 49–54 (2014)
- d’Humières, D., Ginzburg, I., Krafczyk, M., Lallemand, P., Luo, L.S.: Multiple-relaxation-time lattice boltzmann models in three dimensions. *Philos Trans Royal Soc London Serv: Maths Phys Eng Sci* **360**(1792), 437–451 (2002)
- Dou, Z., Zhou, Z.-F.: Numerical study of non-uniqueness of the factors influencing relative permeability in heterogeneous porous media by lattice boltzmann method. *Int. J. Heat Fluid Flow* **42**, 23–32 (2013)
- Dullien, F.A.L., Dong, M.: Experimental determination of the flow transport coefficients in the coupled equations of two-phase flow in porous media. *Transp. Porous Media* **25**(1), 97–120 (1996)
- Gharbi, O., Blunt, M.J.: The impact of wettability and connectivity on relative permeability in carbonates: a pore network modeling analysis. *Water Resour Res* (2012). <https://doi.org/10.1029/2012WR011877>
- Gunstensen, A.K., Rothman, D.H., Zaleski, S., Zanetti, G.: Lattice boltzmann model of immiscible fluids. *Phys. Rev. A* **43**(8), 4320–4327 (1991)
- Guo, Z., Zheng, C.: Analysis of lattice boltzmann equation for microscale gas flows: relaxation times, boundary conditions and the knudsen layer. *Int J Comput Fluid Dyn* **22**(7), 465–473 (2008)

- Guo, Z.L., Zheng, C.G., Shi, B.C.: An extrapolation method for boundary conditions in lattice boltzmann method. *Phys. Fluids* **14**(6), 2007–2010 (2002)
- Guo, Y., He, X., Huang, W., Wang, M.: Microstructure effects on effective gas diffusion coefficient of nanoporous materials. *Transp. Porous Media* **126**(2), 431–453 (2019)
- Ha, J., Kim, H.Y.: Capillarity in soft porous solids. *Annu Rev Fluid Mech* **52**, 263–284 (2020)
- Hughes, R.G., Blunt, M.J.: Pore scale modeling of rate effects in imbibition. *Transp. Porous Media* **40**(3), 295–322 (2000)
- Huppert, H.E., Neufeld, J.A.: The fluid mechanics of carbon dioxide sequestration. *Annu Rev Fluid Mech* **46**, 255–272 (2014)
- Jiang, F., Tsuji, T.: Estimation of three-phase relative permeability by simulating fluid dynamics directly on rock-microstructure images. *Water Resour. Res.* **53**(1), 11–32 (2017)
- Kang, Q.J., Lichtner, P.C., Viswanathan, H.S., Abdel-Fattah, A.I.: Pore scale modeling of reactive transport involved in geologic CO₂ sequestration. *Transp. Porous Media* **82**(1), 197–213 (2010)
- Krevor, S.C.M., Pini, R., Zuo, L., Benson, S.M.: Relative permeability and trapping of CO₂ and water in sandstone rocks at reservoir conditions. *Water Resour Res* (2012). <https://doi.org/10.1029/2011WR010859>
- Latva-Kokko, M., Rothman, D.H.: Diffusion properties of gradient-based lattice boltzmann models of immiscible fluids. *Phys. Rev. E* **71**(5), 056702 (2005)
- Liu, H., Valocchi, A.J., Werth, C., Kang, Q., Oostrom, M.: Pore-scale simulation of liquid CO₂ displacement of water using a two-phase lattice Boltzmann model. *Adv. Water Resour.* **73**, 144–158 (2014)
- Liu, T., Jin, X., Wang, M.: Critical resolution and sample size of digital rock analysis for unconventional reservoirs. *Energies* **11**(7), 1798 (2018)
- Liu, T., Zhang, S., Wang, M.: Does rheology of Bingham fluid influence upscaling of flow through tight porous media? *Energies* **14**(3), 680 (2021)
- Mehmani, A., Kelly, S., Torres-Verdín, C.: Leveraging digital rock physics workflows in unconventional petrophysics: A review of opportunities, challenges, and benchmarking. *J. Petrol. Sci. Eng.* **190**, (2020)
- Mostaghimi, P., Blunt, M.J., Bijeljic, B.: Computations of absolute permeability on micro-CT images. *Math. Geosci.* **45**(1), 103–125 (2013)
- Pan, C., Luo, L.-S., Miller, C.T.: An evaluation of lattice Boltzmann schemes for porous medium flow simulation. *Comput. Fluids* **35**(8–9), 898–909 (2006)
- Parlange, J.Y.: Water transport in soils. *Annu. Rev. Fluid Mech.* **12**, 77–102 (1980)
- Shi, Y., Tang, G.H.: Relative permeability of two-phase flow in three-dimensional porous media using the lattice Boltzmann method. *Int. J. Heat Fluid Flow* **73**, 101–113 (2018)
- Sukop, M.C., Or, D.: Lattice boltzmann method for modeling liquid-vapor interface configurations in porous media. *Water Resour Res* (2004). <https://doi.org/10.1029/2003WR002333>
- Vilarrasa, V., Bolster, D., Dentz, M., Olivella, S., Carrera, J.: Effects of CO₂ compressibility on CO₂ storage in deep saline aquifers. *Transp. Porous Media* **85**(2), 619–639 (2010)
- Wang, J., Wang, M., Li, Z.: A lattice boltzmann algorithm for fluid-solid conjugate heat transfer. *Int. J. Therm. Sci.* **46**(3), 228–234 (2007a)
- Wang, M., Wang, J., Chen, S.: Roughness and cavitations effects on electro-osmotic flows in rough microchannels using the lattice poisson-boltzmann methods. *J. Comput. Phys.* **226**(1), 836–851 (2007b)
- Wang, F., Liu, T., Lei, W., Zhao, Y., Li, B., Yang, G., Liu, Y., Wang, M.: Dynamic analysis of deformation and start-up process of residual-oil droplet on wall under shear flow. *J. Petr Sci Eng* **199**, 108335 (2021)
- Xie, C., Lei, W., Wang, M.: Lattice Boltzmann model for three-phase viscoelastic fluid flow. *Phys. Rev. E* **97**(2), 023312 (2018a)
- Xie, C., Lv, W., Wang, M.: Shear-thinning or shear-thickening fluid for better EOR? - A direct pore-scale study. *J. Petrol. Sci. Eng.* **161**, 683–691 (2018b)
- Xu, Z., Liu, H., Valocchi, A.J.: Lattice Boltzmann simulation of immiscible two-phase flow with capillary valve effect in porous media. *Water Resour. Res.* **53**(5), 3770–3790 (2017)
- Yi, J., Xing, H., Wang, J., Xia, Z., Jing, Y.: Pore-scale study of the effects of surface roughness on relative permeability of rock fractures using lattice boltzmann method. *Chem Eng Sci* **209**, 115178 (2019)
- Yiotis, A.G., Psihogios, J., Kainourgiakis, M.E., Papaioannou, A., Stubos, A.K.: A lattice Boltzmann study of viscous coupling effects in immiscible two-phase flow in porous media. *Colloids Surf Physicochem Eng Aspect* **300**(1–2), 35–49 (2007)
- Yoon, H., Dewers, T.A.: Nanopore structures, statistically representative elementary volumes, and transport properties of chalk. *Geophys. Res. Lett.* **40**(16), 4294–4298 (2013)
- Yu, Z., Fan, L.S.: Multirelaxation-time interaction-potential-based lattice boltzmann model for two-phase flow. *Phys Rev E* **82**(4), 046708 (2010)

- Zhao, H., Ning, Z., Kang, Q., Chen, L., Zhao, T.: Relative permeability of two immiscible fluids flowing through porous media determined by lattice boltzmann method. *Int. Commun. Heat Mass Transfer* **85**, 53–61 (2017)
- Zhao, J., Kang, Q., Yao, J., Viswanathan, H., Pawar, R., Zhang, L., Sun, H.: The effect of wettability heterogeneity on relative permeability of two-phase flow in porous media: a lattice boltzmann study. *Water Resour. Res.* **54**(2), 1295–1311 (2018)

Publisher's Note Springer Nature remains neutral with regard to jurisdictional claims in published maps and institutional affiliations.